Cell Communication and Signaling

RESEARCH

Open Access

Targeting the ERK1/2 and p38 MAPK pathways attenuates Golgi tethering factor golgin-97 depletion-induced cancer progression in breast cancer

Yu-Chin Liu[1], Tsung-Jen Lin[1,2], Kowit-Yu Chong[3,4,5,6], Guan-Ying Chen[1], Chia-Yu Kuo[1], Yi-Yun Lin[7], Chia-Wei Chang[7], Ting-Feng Hsiao[7], Chih-Liang Wang[8,9], Yo-Chen Shih[7] and Chia-Jung Yu[1,7,9,10*]

Abstract

Background The Golgi apparatus is widely considered a secretory center and a hub for different signaling pathways. Abnormalities in Golgi dynamics can perturb the tumor microenvironment and influence cell migration. Therefore, unraveling the regulatory network of the Golgi and searching for pharmacological targets would facilitate the development of novel anticancer therapies. Previously, we reported an unconventional role for the Golgi tethering factor golgin-97 in inhibiting breast cell motility, and its downregulation was associated with poor patient prognosis. However, the specific role and regulatory mechanism of golgin-97 in cancer progression in vivo remain unclear.

Methods We integrated genetic knockout (KO) of golgin-97, animal models (zebrafish and xenograft mice), multi-omics analysis (next-generation sequencing and proteomics), bioinformatics analysis, and kinase inhibitor treatment to evaluate the effects of golgin-97 KO in triple-negative breast cancer cells. Gene knockdown and kinase inhibitor treatment followed by qRT–PCR, Western blotting, cell viability, migration, and cytotoxicity assays were performed to elucidate the mechanisms of golgin-97 KO-mediated cancer invasion. A xenograft mouse model was used to investigate cancer progression and drug therapy.

Results We demonstrated that golgin-97 KO promoted breast cell metastasis in zebrafish and xenograft mouse models. Multi-omics analysis revealed that the Wnt signaling pathway, MAPK kinase cascades, and inflammatory cytokines are involved in golgin-97 KO-induced breast cancer progression. Targeting the ERK1/2 and p38 MAPK pathways effectively attenuated golgin-97-induced cancer cell migration, reduced the expression of inflammatory mediators, and enhanced the chemotherapeutic effect of paclitaxel in vitro and in vivo. Specifically, compared with the paclitaxel regimen, the combination of ERK1/2 and p38 MAPK inhibitors significantly prevented lung metastasis and lung injury. We further demonstrated that hypoxia is a physiological condition that reduces golgin-97 expression in cancer, revealing a novel and potential feedback loop between ERK/MAPK signaling and golgin-97.

Conclusion Our results collectively support a novel regulatory role of golgin-97 in ERK/MAPK signaling and the tumor microenvironment, possibly providing new insights for anti-breast cancer drug development.

Keywords Golgi, Golgin-97, Breast cancer, MAPK signaling, Metastasis, Inflammatory cytokine

*Correspondence:
Chia-Jung Yu
yucj1124@mail.cgu.edu.tw; yucj1124@gmail.com
Full list of author information is available at the end of the article

Introduction

Breast cancer is the most common type of cancer in female patients and the second leading cause of death among women overall [1]. Triple-negative breast cancer (TNBC) has been shown to have a higher incidence of metastasis, a poorer prognosis, and poorer overall survival than other subtypes of breast cancer [2]. TNBC lacks the expression of the sensitive therapeutic markers estrogen receptor, progesterone receptor, and human epidermal growth factor receptor 2, leading to the ineffectiveness of endocrine therapy. Systemic chemotherapy with anthracyclines and taxanes is the most common first-line treatment modality [3]. However, anticancer drug resistance, off-target toxicity, and complications, including pneumonia with severe inflammation, are major obstacles to the development of cancer chemotherapy regimens [4–6]. Although the possible molecular mechanisms of TNBC tumor growth, metastasis, and therapy have been increasingly revealed, their clinical application is still limited. Thus, identifying new molecular targets for predicting clinical prognosis and finding effective strategies for treating TNBC are crucial.

The Golgi apparatus is the trafficking hub that regulates the anterograde transport of modified proteins and lipids or retrieves extracellular proteins through retrograde transport from endosomes [7]. There is growing evidence that the Golgi apparatus is a hub for different signaling pathways [8–10]. Several Golgi-localized proteins have recently been reported to be involved in the function of the Golgi and are related to the regulation of cancer cell migration and invasion [10, 11]. Golgin-97, localized at the *trans*-Golgi network (TGN), is a coiled-coil protein first identified in Sjogren's syndrome patients [12]. Golgin-97 maintains Golgi integrity and acts as a tethering molecule that mediates the vesicular trafficking of specific cargoes (such as E-cadherin) [13–15]. Golgin-97 expression is significantly lower in invasive ductal breast cancer than in ductal carcinoma in situ [16]. Low expression of golgin-97 has also been positively associated with poor overall survival in patients with breast, lung, and ovarian cancers, supporting a suppressive role of golgin-97 in regulating cancer progression. We then revealed a noncanonical role of golgin-97 in suppressing TNBC cell motility through the modulation of NF-κB activity in vitro [17]. Unfortunately, the inhibition of NF-κB alone is insufficient to induce pronounced apoptosis in tumor cells, and long-term treatment with NF-κB inhibitors influences normal cell function, leading to severe systemic toxicity and immunosuppression [18]. Additionally, whether and how golgin-97 depletion promotes cancer metastasis in vivo and the mechanisms affecting golgin-97 downregulation in breast cancer remain unclear.

In this study, we established a cell line with stable golgin-97 depletion via CRISPR–Cas9 gene knockout (KO) and demonstrated that golgin-97 depletion promoted MDA-MB-231 cell migration and metastasis. Multi-omics analysis and functional characterization demonstrated the therapeutic potential of p38 MAPK inhibitors and ERK1/2 inhibitors in golgin-97 KO-induced cancer progression in vitro and in vivo, confirming their biological importance in breast cancer and anticancer drug development.

Materials and methods

Cell culture, chemical reagents, and chemotherapy drugs

The TNBC cell line MDA-MB-231 was purchased from the American Type Culture Collection (Manassas, Virginia). Golgin-97 KO MDA-MB-231 cells were generated via CRISPR–Cas9 gene KO in our laboratory. Both wild-type MDA-MB-231 (hereafter referred to as MDA-MB-231) cells and golgin-97 KO MDA-MB-231 cells were cultured in Dulbecco's modified Eagle's medium (DMEM) (Gibco, Waltham, MA, USA) containing 10% FBS (Gibco), 1% penicillin/streptomycin (Gibco), and 1% L-glutamine (Gibco). SB203580, U0126, and paclitaxel were purchased from MedChemExpress (Monmouth Junction, NJ, USA). Cobalt chloride ($CoCl_2$) was purchased from Sigma (St. Louis, MO, USA).

CRISPR–Cas9 gene deletion

Golgin-97$^{-/-}$ KO MDA-MB-231 breast cancer cells were generated with an optimized single-guide RNA (sgRNA; human golgin-97, accession no. NM_002077.3) and the Cas9 expression plasmid pRGEN-Cas9-CMV (ToolGen, Seoul, Korea). Details for establishing cell lines with golgin-97 KO are described in Appendix S1 (available online).

Cancer metastasis in the zebrafish model

The zebrafish xenotransplantation procedure was described previously [19]. Briefly, 24 h postfertilization (hpf), zebrafish embryos of the wild-type Tübingen strain were dechorionated and anesthetized in E3 medium containing phenylthiourea and tricaine before cell injection. MDA-MB-231 cells (control or golgin-97 KO) were labeled with the lipophilic fluorochrome CM-DiI (Invitrogen, Waltham, MA, USA). Stained cells were injected into the yolk sacs of zebrafish embryos via a microinjector according to the instruction manual. The injected zebrafish were maintained in E3 medium. Images of the zebrafish were acquired with a Z16 APO microscope using a Leica DFC490 color camera system.

Next-generation sequencing (NGS) and bioinformatic analysis

Total RNA was extracted from MDA-MB-231 and golgin-97 KO cells via TRIzol Reagent (Invitrogen, Waltham, MA, USA) according to the instruction manual. NGS was carried out via Illumina's sequencing-by-synthesis technology (Illumina, USS) as described previously [20]. For pathway enrichment analysis, the differentially expressed genes (DEGs) whose expression was altered twofold in golgin-97 KO cells compared with that in MDA-MB-231 cells were subjected to pathway analysis via DAVID Bioinformatics Resources 6.7 (https://david-d.ncifcrf.gov/home.jsp) and QIAGEN Ingenuity Pathway Analysis (IPA) software.

Quantitative proteomic analysis of the differential proteome resulting from golgin-97 KO

Protein extracts prepared from MDA-MB-231 and golgin-97 KO cells were digested with trypsin, chemically labeled with a tandem mass tag (TMT), and then subjected to two-dimensional liquid chromatography–tandem mass spectrometry (2D LC–MS/MS). The details for protein identification and quantification via mass spectrometry are provided in Appendix S1 (available online).

Small interfering RNA (siRNA) transfection

siRNAs targeting p38 MAPK, ERK1/2 and golgin-97 were purchased from Thermo Fisher Scientific or Dharmacon and used for gene knockdown with Lipofectamine RNAiMAX reagents (Invitrogen, Grand Island, NY, USA) according to the manufacturer's instructions. The sequences of the siRNAs used in this study are listed in Table S1.

Cell viability assay

Cell viability was determined by using a Cell Counting Kit-8 (CCK-8) assay (TEN-CCK8) (BIOTOOLS Co., Ltd., New Taipei City, Taiwan). The detailed methods of the cell viability assay are available in Appendix S1 (available online).

Cell and animal tissue RNA extraction and quantitative RT–PCR

Total RNA was extracted from cells or tumor tissue, and cDNA was prepared for qRT–PCR as described previously [17]. The sequences of the primers used in this study are listed in Table S2.

Western blotting

The detailed Western blotting methods are available in Appendix S1. The primary antibodies used included anti-golgin-97 (13192S), anti-IκBα (4814S), anti-p38 (8690S), anti-phospho-ERK1/2 (9101S), anti-cleaved caspase-3 (#9661) and anti-caspase-3 (#9662), which were purchased from Cell Signaling Technology (Danvers, MA, USA). The anti-ERK (sc-93) antibody was purchased from Santa Cruz (DT, USA). Anti-phospho-p38 (09–272) and anti-β-actin (MAB1501) antibodies were obtained from Merck Millipore (Burlington, MA, USA). The anti-HIF1α (GTX127309) antibody was purchased from GeneTex (Irvine, CA, USA). The anti-TGN46 antibody was purchased from Bio-Rad (Hercules, CA, USA).

Wound healing migration assay

The cell migration ability was analyzed via a wound healing assay. The detailed methods are available in Appendix S1 (available online).

Animal model of metastasis

This study was approved by the Institutional Animal Care and Use Committee of Chang Gung University (CGU107–228). Four-week-old female immunodeficient nonobese diabetic/SCID (NOD. CB17-*Prkdc*^{scid}/JNarl) mice were purchased from the National Laboratory Animal Center (Taipei, Taiwan) to establish the tail vein injection and orthotopic inoculation models as described in Appendix S1 (available online).

Immunohistochemical (IHC) analysis

The detailed IHC methods are available in Appendix S1.

Statistical analysis

All experiments were performed at least in triplicate, and the data are presented as the means ± standard deviations (SDs). Prism 8.0 (GraphPad Software) statistical software packages were used for data analysis. Unpaired *t* tests, one-way ANOVA, two-way ANOVA, and log-rank tests were used for comparisons between the control and experimental groups. A *P* value less than 0.05 ($P < 0.05$) was considered to indicate significance.

Results

Golgin-97 KO modulates the malignancy of breast cancer cells *in vivo*

Our previous studies revealed that golgin-97 knockdown promotes NF-κB activation and leads to increased migration/invasion of breast cancer cells [17]. Herein, we applied CRISPR–Cas9 to generate four clonal golgin-97 KO cell lines (Fig. S1A). We confirmed that the expression levels of IκBα and TGN46 were reduced, accompanied by increased migration and invasion of 2–9 and 2–20 KO cells (Fig. S1B). Therefore, to verify the effects of golgin-97 depletion on cancer metastasis in vivo,

cancer cells were injected into the perivitelline cavity of fertilized zebrafish embryos. Four experiments were conducted with ten fish per group, resulting in a total of more than 30 zebrafish per group. The results indicated that 20% of the MDA-MB-231 cells had metastasized by day one, an increase of 24% according to subsequent observations. In comparison, golgin-97 KO (2–9) cells presented a greater metastasis rate, beginning at 46% on day one, peaking at 52% on day two, and subsequently declining to 36% on day three. Golgin-97 KO (2–20) cells presented lower rates of metastasis, with rates of 17%, 30%, and 34%, respectively. In the present study, we present the quantitative results obtained on day two, as shown in Fig. 1B. CM-DiI staining further revealed that the number of cancer cell clusters spread distal to the primary site was significantly greater in fish injected with golgin-97 KO cells than in those injected with MDA-MB-231 cells (Fig. 1A and B). Furthermore, when MDA-MB-231 and

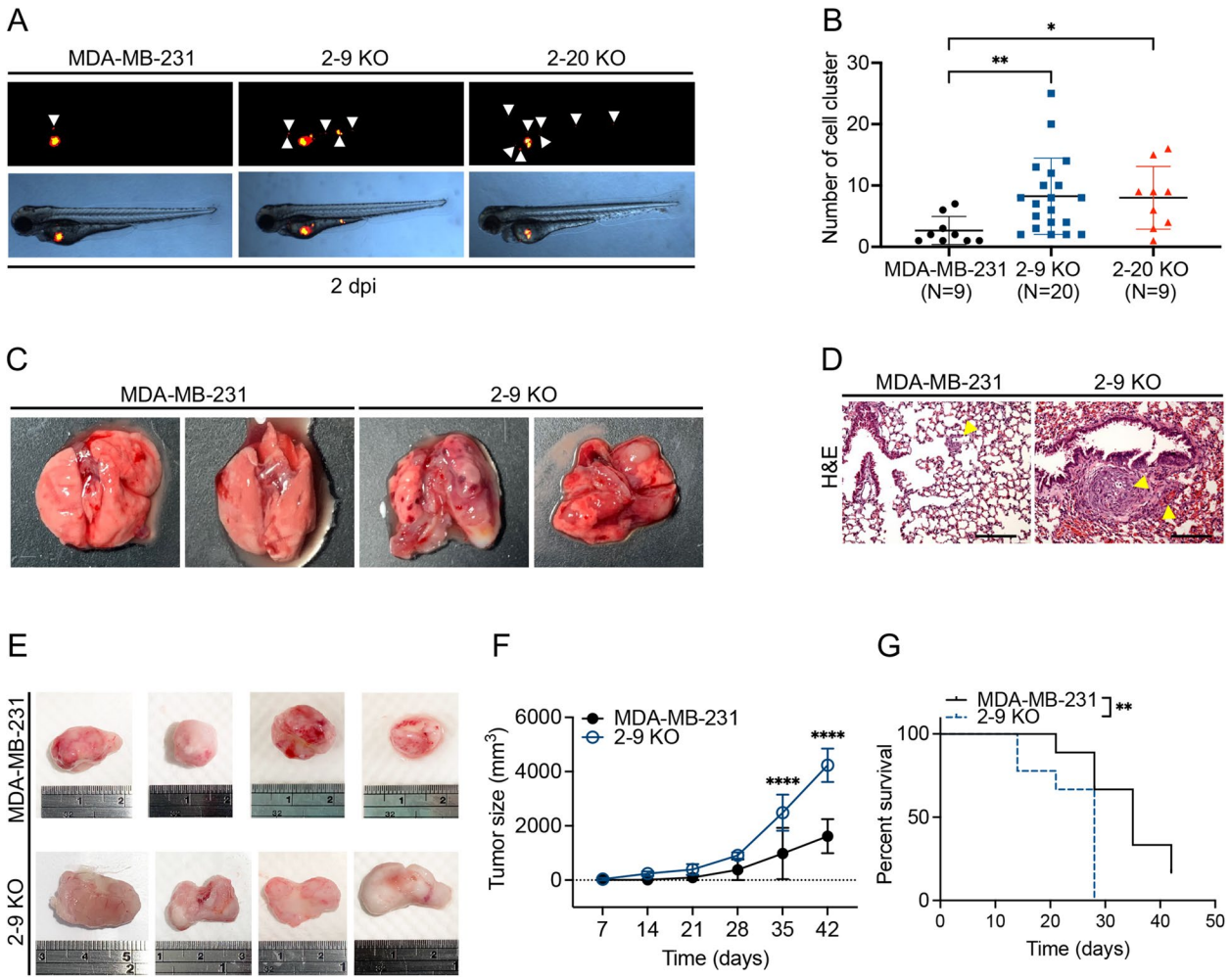

Fig. 1 Golgin-97 KO modulates the malignancy of breast cancer cells in vivo. **A** Representative images showing that MDA-MB-231 and golgin-97 KO cells were injected into the perivitelline cavity of zebrafish embryos and analyzed with a dissecting microscope. The location of the cancer cells is indicated in red on bright field images of zebrafish. The white arrows indicate dispersed breast cancer cells. **B** Quantification of the number of cell clusters on the basis of the acquired images in Fig. 1A. Each dot represents one live fish for image analysis. The quantitative data were analyzed via one-way ANOVA. **C** Representative images of lung metastases formed from MDA-MB-231 and 2–9 KO cell-derived NOD/SCID mice on day 28 after tail vein injection. **D** Representative IHC images with H&E staining of lung metastases. Scale bars, 100 μm. The yellow arrows delineate the tumor region. **E** Representative images showing the tumor sizes on day 42 after the injection of MDA-MB-231 and 2–9 KO cells into the right middle mammary fat pads of the mice. **F** Tumor growth was monitored at the indicated times after the injection of MDA-MB-231 and 2–9 KO cells, and tumor growth curves were constructed. The data were analyzed via two-way ANOVA. **G** Compared with those injected with MDA-MB-231 cells, NOD/SCID mice injected with golgin-97 KO cells exhibited poor survival ($n = 9$ mice per group). Kaplan–Meier plots of mouse survival using a standard tumor volume of 300 mm^3 as a criterion for euthanasia. *P* values were determined via the log-rank test. The data are presented as the means ± SDs (*$p < 0.05$; **$p < 0.01$; ****, $P < 0.0001$)

golgin-97 KO cells were injected into the lateral tail veins of immunodeficient NOD/SCID mice, a trend toward the formation of lung foci was observed in golgin-97 KO cell-injected mice, suggesting that golgin-97 KO breast cancer cells have a greater rate of survival and colonization success (Fig. 1C). H&E staining revealed that golgin-97 KO increased the tumor cell density and resulted in the formation of large nodules in the stroma (Fig. 1D). Thus, these differences in cell morphology and organization suggest that golgin-97 KO enhances the invasive potential of cancer. In addition, the orthotopic mouse model demonstrated that the tumors derived from golgin-97 KO cells were significantly larger than the tumors derived from MDA-MB-231 cells (Fig. 1E). Quantitative analysis revealed a significant increase in tumor size in golgin-97 KO cell-injected mice on day 35 (Fig. 1F). As expected, the survival time of golgin-97 KO mice was shorter than that of MDA-MB-231 mice (Fig. 1G). These results collectively support the suppressive role of golgin-97 in the tumor growth and metastatic progression of breast cancer in vivo.

Multi-omics reveals the involvement of key factors in golgin-97 KO-mediated breast cancer progression

To identify signaling pathways containing potential therapeutic targets regulated by golgin-97, NGS and quantitative proteomic analysis were applied. Analysis of the intersection of the two resulting datasets revealed that 783 DEGs were significantly upregulated, with a twofold change in expression, in two golgin-97 KO cell lines (2–9 KO and 2–20 KO) compared with that in MDA-MB-231 cells (Fig. 2A). The IPA results suggested that several upstream regulators and pathway networks, including cytokines (IL-1β, TNF), growth factors (BMP4, AGT), signal transduction factors (p38 MAPK), and transcription factors (NF-κB-RelA), are significantly involved in the upregulation of these 783 DEGs (Fig. 2B and Table 1). The RT–qPCR results verified that the expression levels of three DEGs (IL-1β, IL-6, and MMP1) regulated by the abovementioned key regulators were significantly higher in golgin-97 KO cells than in MDA-MB-231 cells (Fig. 2C). Additionally, DAVID bioinformatic analysis revealed that the DEGs upregulated by golgin-97 KO mediate biological processes such as the Wnt signaling pathway, the MAPK cascade, wound healing, and the cellular response to IL-1 (Fig. 2D). We also performed TMT-based quantitative proteomics to identify 7271 quantified proteins in golgin-97 KO and MDA-MB-231 cells. Using 1.5 SDs of the fold change as a cutoff value, we identified 219 proteins upregulated (1.44-fold increase) by golgin-97 KO. Consistent with the NGS analysis results, our combined proteomic analysis/IPA revealed that TGFβ1, EHF, TNF, JUNB, and IL-1α were the main activators upregulated in response to golgin-97 KO (Fig. 2E and Table S3). These results were consistent with our earlier study in which we utilized a quantitative proteomics approach to establish a dataset that profiles the secreted proteome, termed the secretome, which comprises 1,872 identified and quantified proteins from the conditioned media of MDA-MB-231 cells, both with and without golgin-97 knockdown. Among the proteins identified, 103 exhibited a 1.5-fold change in secretion levels. Of these proteins, 88, including IL-6, IL-8, GM-CSF, TL1A, PLAU, and ISG15, exhibited upregulation, whereas 15 proteins demonstrated downregulation in the golgin-97-knockdown cells in comparison to the control cells. Gene Ontology analysis revealed that these 103 proteins were associated primarily with processes associated with the wound response, cell migration, cellular localization, cellular motility, and immune system functions (Fig. S2). Our previous study also revealed that conditioned medium from golgin-97-knockdown cells promoted recipient cell migration and invasion, whereas an NF-κB inhibitor reduced golgin-97-knockdown-induced TNBC cell motility [17]. Taken together, these results suggest that golgin-97 KO promotes cancer progression primarily by modulating inflammatory responses and Wnt/MAPK signaling in breast cancer cells.

Golgin-97 KO induces tumor progression and metastasis accompanied by lung colonization and inflammatory cell infiltration

In this study, we measured higher levels of murine TGFβ and the proinflammatory cytokine TNFα in primary tumors derived from golgin-97 KO cells than in those derived from MDA-MB-231 cells (Fig. 3A), indicating that golgin-97 KO may promote tumor growth and metastasis by modulating the tumor microenvironment. Moreover, IHC analysis of primary tumors revealed increased expression of the proliferation marker Ki67 and the macrophage/monocyte marker CD68 in golgin-97 KO tumors (Fig. 3B). To investigate whether golgin-97 influences macrophage polarization in the tumor microenvironment of breast cancer, we conducted a co-culture experiment involving cancer cells and PMA-induced human leukemia monocytic THP-1 cells. Our results indicated that both parental MDA-MB-231 cells and golgin-97 KO cells induced a mix of pro-inflammatory and anti-inflammatory factors production, enabling macrophages to exhibit characteristics of both M1 and M2 polarization. This finding aligns with recent studies that highlight the complexity of macrophage polarization, where cells can display traits of both M1 and M2 phenotypes [21, 22]. To further examine the effect of golgin-97 on macrophage polarization and function within the tumor microenvironment associated with breast cancer

Table 1 The IPA bioinformatics analysis reveals the upstream regulators for 783 up-regulated genes induced by golgin-97 knockout

Upstream regulator	Molecule type	*p* value	Target molecules in dataset
IL1B	Cytokine	1.00E-08	ACKR2,ADAMTS1,ANGPTL4,APOB,ASS1,BMF,C1R,C3,CABP1,CCL11,CCL20,CCL24,CEBPB,CHST6,CSF3,CXCL1,CYP19A1,CYP1B1,DUSP1,EBI3,ELF3,ENG,FPR2,GDF15,HAS1,HLAA,IER3,IER5L,IL18,IL18R1,IL1A,IL1B,IL6,IL7R,INHBA,IRAK3,ITGB3,ITPKB,LCN2,LDHA,LOXL4,MAFA,MAPT,MEF2B,MEFV,METRNL,MMP1,MMP3,MUC2,MYLK3,NOS3,PAPPA,PLXDC2,PTGS1,PTGS2,REN,SAA2,SCX,SERPINB2,SERPINB3,SHH,SLC1A3,SOCS1,SRGN,ST18,TAP2,TGM2,TNFRSF11B,TREM1,VSNL1,WNT5A,ZC3H12A
BMP4	Growth factor	1.15E-08	CCL11,CDH5,CEBPB,CSF3,CYP19A1,DIO2,DLX3,DLX4,ELF3,HSD3B1,IL6,INHBA,LEF1,LEFTY1,MMP3,PGF,PITX2,PRKCH,PRR5,SHH,SNAI1,SPINT1,TAL1,TFAP2C,TGM2,TNFRSF11B,WNT5A
TNF	Cytokine	1.16E-08	ACKR2,ADAMTS7,ALB,ALDH3A1,ALOX5AP,ANGPTL4,APOA1,AQP3,ASGR1,ASS1,B4GALNT1,BDKRB2,BIK,BMP6,C1QTNF1,C3,CABP1,CCL11,CCL20,CCL24,CCN4,CD207,CD70,CDH11,CDH5,CDO1,CEBPB,CIB2,CMKLR1,CSF3,CXCL1,CYP19A1,CYP1B1,DUSP1,DUSP14,DUSP9,EBI3,ECH1,ELF3,ENG,FAT2,FBXO32,FPR1,FPR2,GDF15,GPRC5B,HAND1,HAS1,HCAR3,HEPACAM,HLAA,IER3,IL18,IL18R1,IL1A,IL1B,IL6,IL7R,INHBA,IRAK3,ITGB3,LAMP3,LCN2,LDHA,LPL,LRIG1,LTBP2,MAFA,MEFV,METRNL,MMP1,MMP3,MUC2,MUC20,NFATC1,NOS3,PAPPA,PCK1,PDGFA,PGF,PLA2G4C,PLXDC2,PTGS1,PTGS2,RAPGEF5,ROBO1,RRAD,SERPINB2,SHH,SLC16A2,SLC1A3,SNAI1,SOCS1,SOX4,SYNGR3,TAPBP,TFAP2C,TG,TGM2,TH,TNFRSF11B,TNNC1,TREM1,TRIM63,UCN2,VIPR1,WNT1,WNT3A,WNT5A,ZC3H12A,ZNF750
P38 MAPK	Group	2.72E-08	ASS1,CCL11,CD70,CDH5,CEBPB,CSF3,CXCL1,CYP19A1,DIO2,DUOX2,DUSP1,FBXO32,FGF21,IER3,IL1A,IL1B,IL6,INHBA,ITGB3,MAL,MMP1,MMP3,MUC2,MYBPH,NFATC1,NOS3,PCK1,PTGS2,RRAD,SERPINB2,SNAI1,TH,TJP2,TNNC1,TREM1,WNT5A
DSCAML1	Other	5.51E-08	ATOH7,BMP6,DNER,EMX1,LHX9,MAPT,NPAS3,NRCAM,NTNG2,PAX5,PCDH17,PDGFA,PRKCH,ROBO2,SHANK1,TUBB4A
NFkB1-RelA	Complex	6.06E-08	CCL11,CCL20,CSF3,CXCL1,IL1B,IL6,LCN2,MMP1,MMP3,PTGS2,TNFRSF11B
AGT	Growth factor	6.53E-08	ADGRE1,AMBP,ANGPTL8,BDKRB2,BMP6,C1QTNF1,C3,CCN4,CDH5,COL4A1,COL4A2,COL6A2,COLEC10,CYP19A1,DIO2,DUSP1,ENG,FGA,GAA,GABBR1,GAS2,GDF15,HSD3B1,IL18,IL18R1,IL1A,IL1B,IL6,ITGB3,ITPKB,LCN2,LGI3,LOXL4,LRP1,LRRC7,LTBP2,LTBP3,MAPT,MMP1,MMP3,MYO7A,NOS3,PDGFA,PGF,PTGS1,PTGS2,PTPN22,REN,ROBO1,SCG2,SERPINB2,SH2D1B,SLC1A1,SOCS1,SOST,SOX4,SPINT1,SUSD5,TH,TNFRSF11B,VTN,XIRP1
Dexa-methasone	Chemical drug	9.83E-08	ABCC6,ACY3,ADAMTS1,AFP,ALB,ALOX5AP,ANGPTL4,APOA1,ATF7IP2,ATP9A,AVPR1B,BDKRB2,BMP5,C12orf42,C3,C8A,CCL11,CCL20,CDH11,CDKN1C,CEBPB,CELF2,CLDN9,CMKLR1,COL4A1,COL4A2,COL6A2,COL7A1,CTSE,CTSW,CXCL1,CYP19A1,CYP1B1,DIO2,DNER,DUSP1,EDA,FAM107A,FBLN1,FBXO32,FGA,FGF21,FOXQ1,FPR2,FSD2,GABBR1,GAS2L2,GBP5,GDF15,GNGT2,GNRH2,HCST,HLAA,HSPA6,IER3,IL18,IL18R1,IL1A,IL1B,IL2RB,IL6,IL7R,INHBA,IRAK3,ITGB3,KCNK3,KLRC4KLRK1/KLRK1,LCN2,LDHA,LEF1,LEFTY1,LPL,LRP1,LSR,LTBP2,MATN1,MATN3,MMP1,MMP3,MUC2,NFATC1,NOS3,NPPC,NTF3,OR51E1,OSBP2,PCK1,PDGFA,PPP1R14C,PTGFRN,PTGS1,PTGS2,PTPN22,RAB37,RPS6KA2,RRAD,SAA2,SAA4,SCG2,SERPINB2,SHH,SLC1A3,SLC2A5,SLC4A1,SNAI1,SOCS1,SRGN,TAP2,TGM2,TLE2,TMEM61,TNFRSF11B,TNS4,TRIM63,TRPM2,TUBB1,UCN2,VIPR1,WNT2,WNT5A,ZC3H12A,ZIC2,ZNF750
DSCAM	Other	1.21E-07	EMX1,KCNJ4,MAPT,NPAS3,NRCAM,NTF3,NTNG2,PAX5,PCDH17,PDGFA,PRKCH,ROBO2,SLC1A1,SYNGR3,TAL1,TUBB4A
CD36	Transmembrane receptor	2.19E-07	ADGRE1,APOA1,APOB,CCL20,COL4A1,CSF3,CXCL1,IL1A,IL1B,IL6,LPL,LRP1,MMP1,MMP3,SERPINB2,TNFRSF11B

(See figure on next page.)

Fig. 2 Multi-omics reveals the involvement of key factors in golgin-97 KO-mediated breast cancer progression. **A** The DEGs between the two golgin-97 KO cell lines and the MDA-MB-231 cells were analyzed via next-generation sequencing (NGS). The Venn diagram shows the 783 overlapping genes upregulated by golgin-97 KO. **B** The graphical summary of the IPA results shows the key molecules and functions of these 783 upregulated genes in golgin-97 KO cells. **C** qRT–PCR analysis of IL-1β, IL-6, and MMP1 mRNA levels in MDA-MB-231 and golgin-97 KO cells. The data are shown as the means ± SDs. **, $P < 0.01$; ***, $P < 0.001$; ****, $P < 0.0001$ based on one-way ANOVA. **D** The biological processes of the 783 genes upregulated by golgin-97 KO were analyzed with the DAVID bioinformatics resource. **E** Quantitative proteomics combined with bioinformatic analysis revealed network and disease-related functions in which the 219 proteins upregulated by golgin-97 KO were involved. The orange octagons, squares, and ovals represent functions, cytokines, and transcriptional regulators, respectively. The orange hourglasses represent canonical pathways. The orange dotted lines indicate activation, and the gray dotted lines indicate unpredicted effects

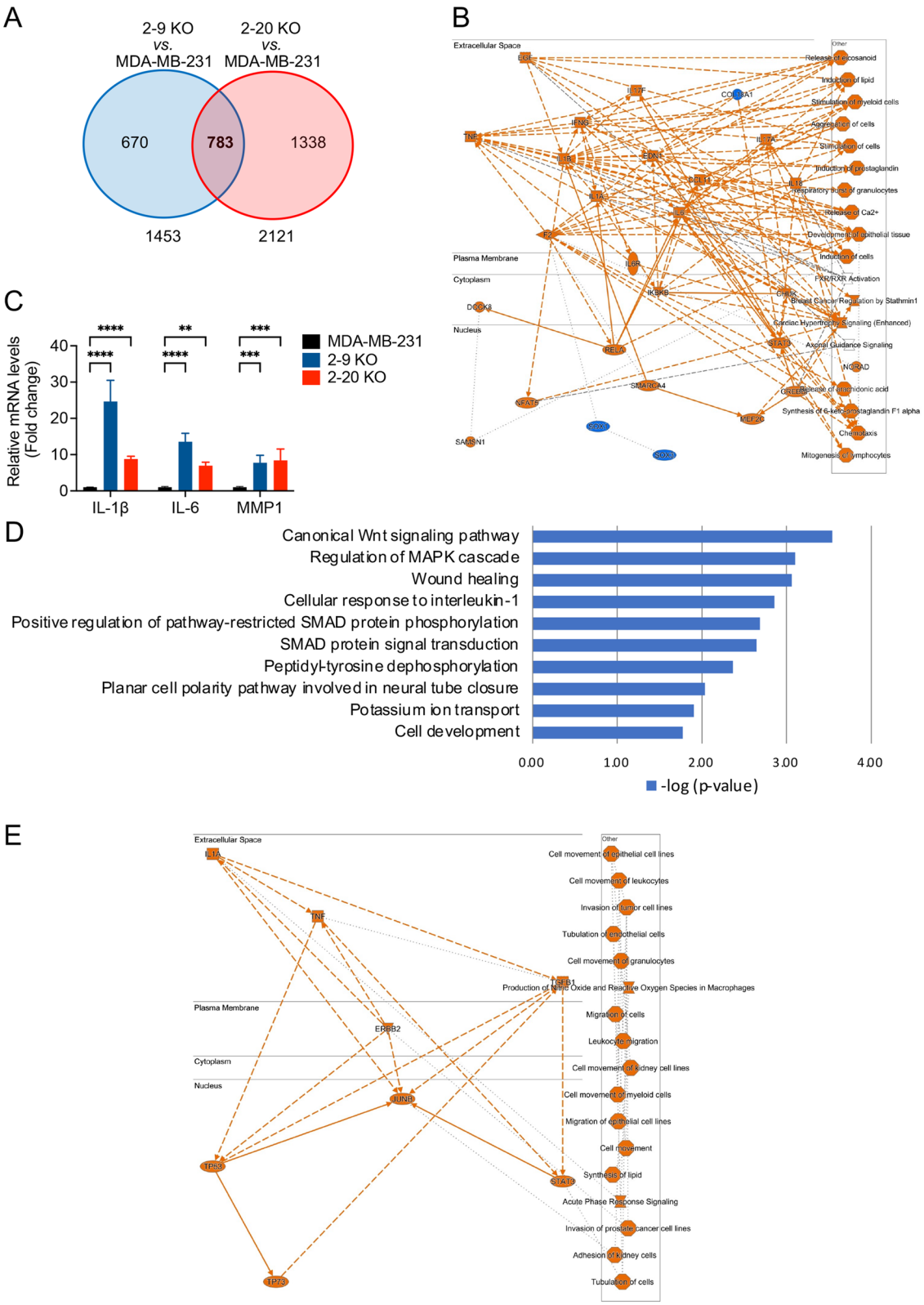

Fig. 2 (See legend on previous page.)

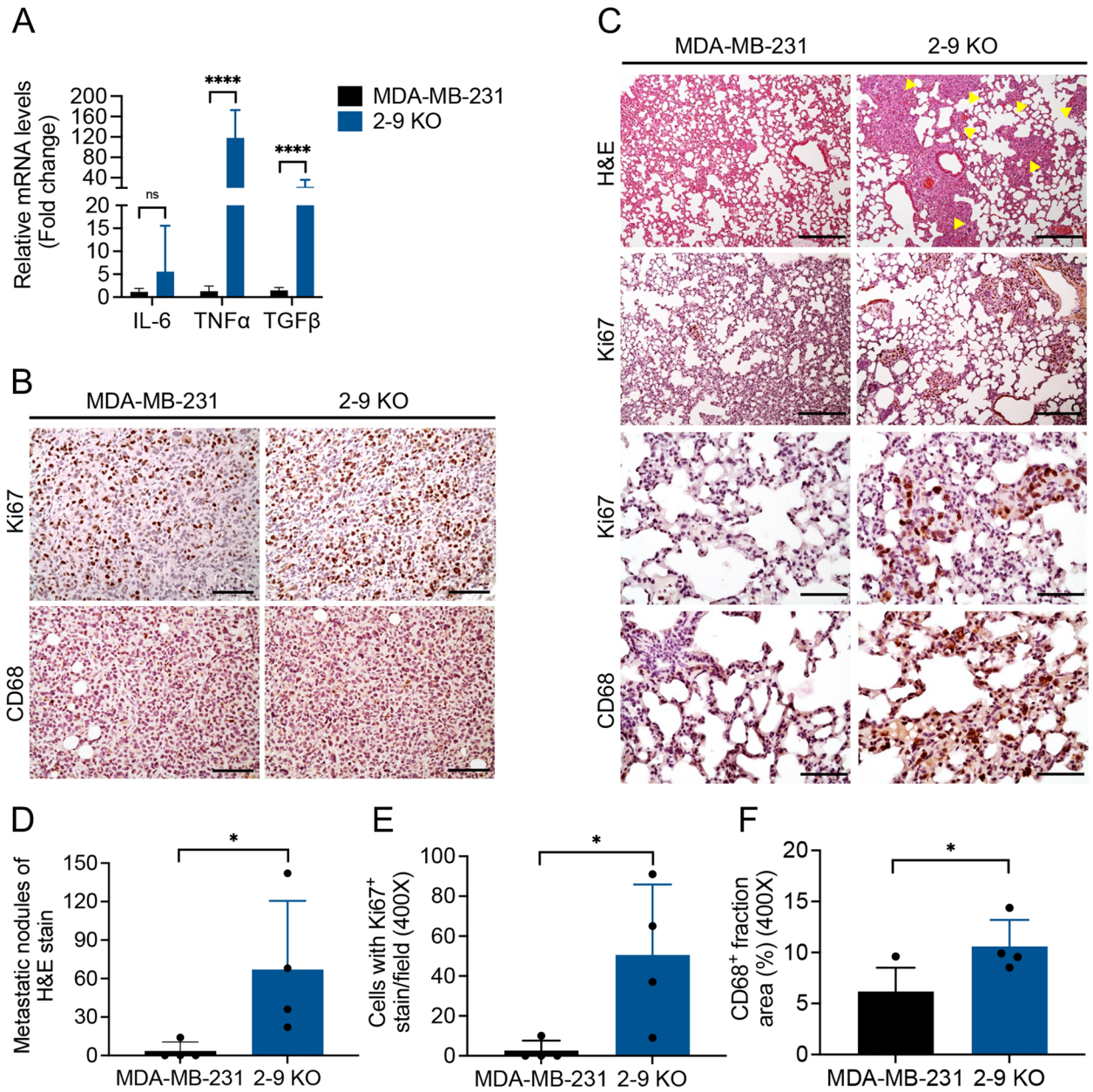

Fig. 3 Golgin-97 KO induces tumor progression and metastasis accompanied by lung colonization and inflammatory cell infiltration. **A** qRT–PCR analysis of murine IL-6, TNFα, and TGFβ mRNA levels in primary tumors from mice ($n = 9$ mice per group). The data are based on an unpaired *t* test. **B** Representative images of IHC staining for Ki67 and CD68 in primary tumors. Scale bars, 100 μm. **C** Representative images of lung metastasis sections with H&E staining and IHC staining with anti-Ki67 and anti-CD68 antibodies. The yellow arrows delineate the tumor region. Scale bars, 200 μm (H&E and Ki67) and 50 μm (Ki67 and CD68). **D-F** Quantification of lung metastatic nodules, Ki67-positive cells, and CD68-positive cells in the MDA-MB-231 and 2–9 KO groups ($n = 4$ mice per group). The quantitative data were analyzed via an unpaired t test. The data are presented as the means ± SDs (*$p < 0.05$; **$p < 0.01$; ****, $P < 0.0001$)

in vivo, we performed an association analysis of golgin-97 gene expression (GOLGA1) with M1 and M2 macrophages in BRCA-Basal (TNBC > 70%) via TIMER2.0 (http://timer.cistrome.org/), an integrated online database that compiles cancer research and immune association data from multiple sources. Our analysis suggested that golgin-97 may be positively correlated with M1 macrophages, as indicated by the CIBERSORT data, but negatively correlated with M2 macrophages, according to findings from the TIDE data (Fig. S3). Together, these observations suggest that the downregulation of golgin-97 in breast cancer cells may increase M2

macrophage polarization through complex communication between multiple cell types in tumor microenvironment. Next, we examined whether golgin-97 KO promotes metastatic tumor cell colonization. H&E staining and Ki67 and CD68 expression were evaluated in lung sections. Quantitative analysis revealed that golgin-97 KO significantly increased the nodule number and lung metastatic colonization, as well as the infiltration of macrophages/monocytes (Fig. 3C-F). These results suggested that golgin-97 KO significantly and positively influences primary tumor colonization and metastasis, an effect that involves proinflammatory factor-controlled interplay between golgin-97 KO cells and stromal cells.

Targeting ERK/MAPK kinase attenuates golgin-97 KO-induced breast cancer malignancy and enhances paclitaxel treatment efficacy

To search for new therapeutic targets to benefit patients with malignancy and chronic inflammation induced by low expression of golgin-97, we conducted an IPA of the 783 upregulated DEGs identified from the intersection of NGS data derived from two golgin-97 KO cell lines. The analysis revealed a total of 629 chemical compounds, including both activators and inhibitors. Notably, when the predicted activation state of inhibition was examined, 36 chemical compounds were identified and subsequently ranked on the basis of a p value of less than 0.05, with the top five compounds documented in Table 2. Among these, we emphasized two leading chemical inhibitors: U0126 (MEK1/2 inhibitor) and SB203580 (p38 MAPK inhibitor). A wound healing assay revealed that golgin-97 KO cells had greater collective migration capacity than did MDA-MB-231 cells. Importantly, SB203580 and U0126 alone or in combination significantly reduced golgin-97 KO-induced cell motility (Fig. 4A). RT–qPCR analysis revealed that U0126 and SB203580 significantly reduced the mRNA expression levels of IL-1β, IL-6, and MMP1 in golgin-97 KO cells (Fig. 4B). Gene-specific silencing via siRNA transfection was further used to confirm the phenomena shown by chemical inhibitor treatment. As shown in Fig. 4C, the mRNA expression levels of IL-1β, IL-6, and MMP1 were decreased by p38 MAPK knockdown. ERK1/2 knockdown reduced the mRNA expression of IL-1β and MMP1 but not that of IL-6. Knockdown of p38 MAPK and ERK1/2 also significantly inhibited the increased cell migration ability induced by golgin-97 depletion in MDA-MB-231 and MCF-7 cells (Fig. 4D-E), and the knockdown efficacy is shown in Fig. S4A-B. Although golgin-97 KO did not promote the proliferation of breast cancer cells in vitro, treatment with U0126 alone or in combination with SB203580 reduced the viability of golgin-97 KO cells and MDA-MB 231 cells after 48 h and 72 h, respectively (Fig. 4F). Paclitaxel (PTX) is the most commonly used chemical agent for the clinical treatment of TNBC, and long-term chemotherapy causes severe side effects in patients [23, 24]. We then tested whether treatment with U0126 or SB203580 as adjuvants with paclitaxel would benefit patients with golgin-97 deficiency. The results of the cell viability assay revealed that treatment with PTX or two-kinase inhibitors (U0126 and SB203580) was cytotoxic to golgin-97 KO cells (Fig. 4G). Notably, combined treatment with these three drugs (U0126 + SB203580 + PTX) significantly resulted in a synergistic effect compared with PTX alone or the combination of U0126 and SB203580 (Fig. 4G). These results suggest that the inhibition of both the ERK1/2 kinase pathway and the p38 MAPK pathway has therapeutic potential for the treatment of breast cancer patients with low expression of golgin-97.

Inhibition of ERK/MAPK kinase is effective in overcoming golgin-97 KO-induced tumor growth and lung metastasis

We next examined the therapeutic potential of ERK1/2 kinase and p38 MAPK inhibitors in an orthotopic mouse model. We observed that treatment with PTX alone, two-kinase inhibitors, or a combination of the three drugs significantly reduced the tumor growth rate and tumor volume, with targeting of ERK1/2 kinase and p38 MAPK enhancing the efficacy of PTX-based chemotherapy. (Fig. 5A-B). Specifically, growth inhibition and survival protection were most pronounced in the kinase inhibitor treatment groups (Fig. 5B-C). To confirm whether

(See figure on next page.)

Fig. 4 Targeting ERK/MAPK kinase attenuates golgin-97 KO-induced breast cancer malignancy and enhances paclitaxel treatment efficacy. **A** Wound healing assay of MDA-MB-231 and 2–9 KO cells treated with vehicle (veh.) control, SB203580 (20 μM), U0126 (20 μM), or SB203580 (20 μM) + U0126 (20 μM) for 17 h (left panel) and quantification of cell migration (right panel). The quantitative data were analyzed via one-way ANOVA. qRT–PCR analysis of IL-1β, IL-6, and MMP1 mRNA levels in 2–9 KO cells treated with inhibitors (**B**) or gene-specific knockdown (**C**) as indicated. The data were analyzed via one-way ANOVA. Wound healing assays with gene-specific knockdown of p38 MAPK and ERK1/2 as indicated were performed on 2–9 KO cells (**D**) and MCF-7 cells (**E**). The data were analyzed via one-way ANOVA. **F** MDA-MB-231 and 2–9 KO cells were treated with vehicle control, SB203580, U0126, or a combination (SB203580 + U0126) for the indicated times, followed by a cell viability assay. **G** 2–9 KO cells were treated with vehicle control, SB203580 + U0126, PTX, or PTX + SB203580 + U0126 for the indicated times, followed by a cell viability assay. The data were analyzed via two-way ANOVA. The data are presented as the means ± SDs. *$p < 0.05$; **$p < 0.01$; ***, $P < 0.001$; ****, $P < 0.0001$. Images from each group in all the wound healing assays were acquired in three random fields of view via microscopy

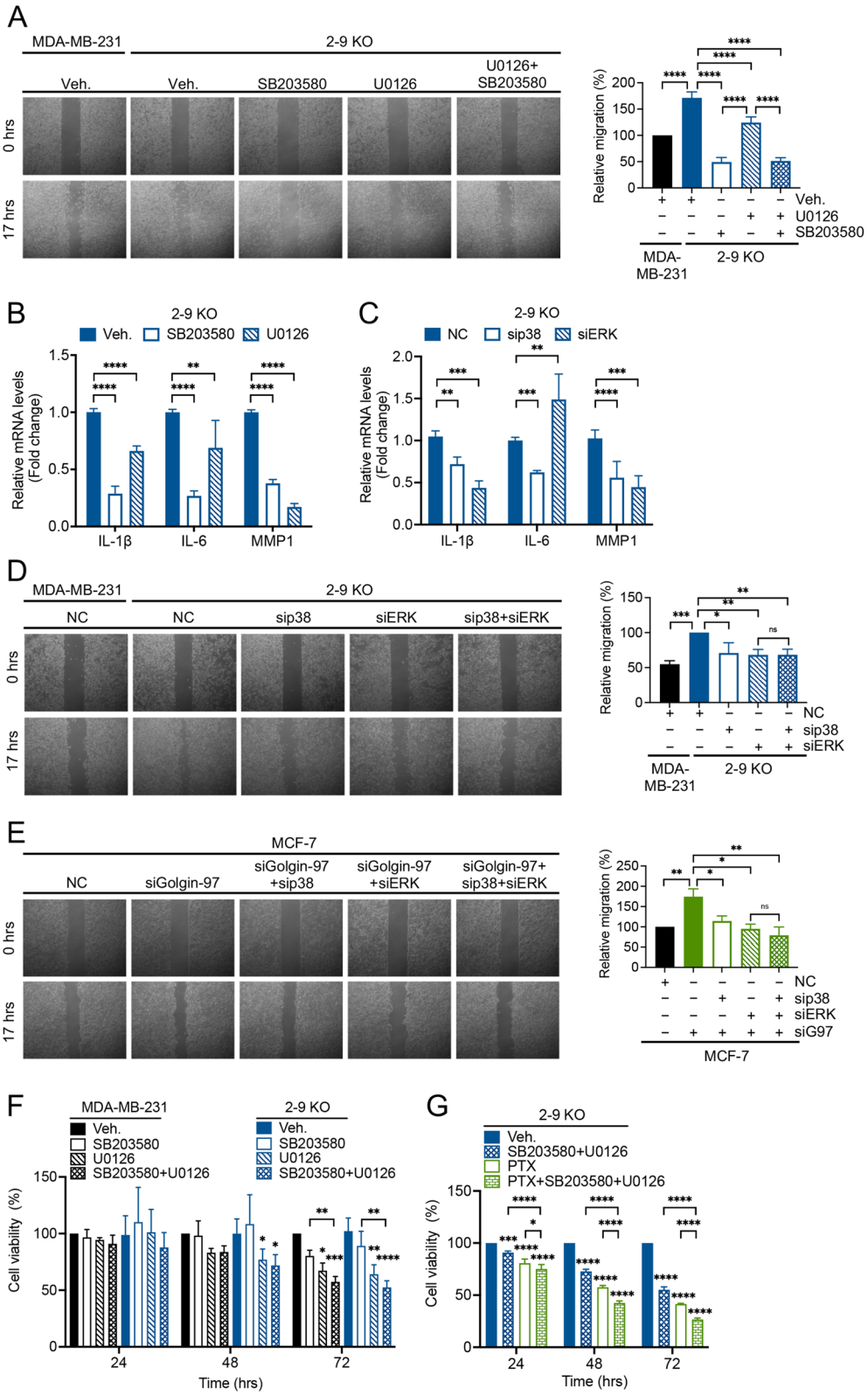

Fig. 4 (See legend on previous page.)

Table 2 Potential chemical inhibitors used to suppress the 783 genes upregulated by golgin-97 knockout

Upstream regulator	Molecule type	Predicted activation state	*p* value	Target molecules in dataset
U0126	Chemical - kinase inhibitor	Inhibited	6.34E-06	ADGRE1,ANGPTL4,AQP3,BMP6,C3,CCL11,CCN4,CDH5,CDKN1C,CEBPB,COL4A1,CSF3,CXCL1,CYP19A1,CYP1B1,DUSP1,GDF15,IER3,IL1A,IL1B,IL6,INHBA,ITGA2B,LPL,MMP1,MMP3,MUC2,MYO7A,NFATC1,NXPH4,PTGS2,REN,SERPINB2,SHH,SOCS1,TAP2,TGM2,TH,TNFRSF11B,ZIC2
SB203580	Chemical - kinase inhibitor	Inhibited	2.38E-05	ALOX5AP,C3,CCL11,CCL20,CD207,CEBPB,CXCL1,CYP1B1,DUOX2,DUSP1,EBI3,FGF21,FOXQ1,FPR2,HAND1,HAS1,HCAR3,HEPACAM,IER3,IL18,IL1A,IL1B,IL6,ITGB3,MMP1,MMP3,MUC2,NOS3,PCK1,PDGFA,PTGS2,SNAI1,TGM2,TNFRSF11B,TREM1
PD98059	Chemical - kinase inhibitor	Inhibited	4.43E-05	ALOX5AP,APOA1,BDH1,C3,CCL11,CCL20,CEBPB,COL4A1,CXCL1,CYP19A1,CYP1B1,DIO2,DUSP1,ENG,FPR2,HAS1,IER3,IL1A,IL1B,IL6,ITGA2B,ITGB3,KLRC2,LDHA,LPL,MMP1,MMP3,MT1F,MUC2,NOS3,PCK1,PDGFA,PTGS2,REN,SERPINB2,SHH,SNAI1,TH,TP73
Aspirin	Chemical drug	Inhibited	1.17E-04	APOA1,BMP6,CDH5,CSF3,CXCL1,ENG,GDF15,IER3,IL18,IL1A,IL1B,IL6,ITPKB,MMP1,PTGS1,PTGS2,SOX4
AS1842856	Chemical reagent	Inhibited	1.20E-04	CXCL1,FBXO32,IL6,MMP1,MMP3,TRIM63

these two kinase inhibitors modulate cancer-associated inflammation in this mouse model, the expression of CD68 and inflammatory mediators in primary tumors was examined. IHC revealed that PTX (PTX alone and three drugs), but not two-kinase inhibitor, significantly reduced CD68 expression (Fig. 5D-E). However, qRT–PCR revealed that the administration of kinase inhibitors alone or in combination with PTX resulted in reduced mRNA expression of murine TNFα and TGFβ (Fig. 5F-G). Compared with that in the vehicle group, the expression of murine TGFβ but not TNFα was lower in the PTX alone group (Fig. 5F-G). Additionally, quantitative analysis of IHCs obtained from lung tissue sections revealed that treatment with two-kinase inhibitors (two-kinase inhibitors alone or three drugs) but not PTX alone resulted in lower levels of human Ki67 expression, indicating a reduction in lung metastatic colonization (Fig. 5H-I). Notably, we observed significant infiltration of CD68 and induction of cleaved caspase-3 expression in lung tissues treated with PTX alone or the three drugs, suggesting that PTX treatment may increase the potential for lung inflammation and lung injury (Fig. 5J-L). These results collectively suggest that ERK1/2 and p38 MAPK inhibitors can effectively treat golgin-97-KO-induced breast cancer malignancy by reducing inflammation at the primary tumor site and inhibiting lung organ metastasis.

Hypoxia mimetics and ERK/MAPK signaling regulate golgin-97 expression in breast cancer

Hypoxia is detected in most solid tumors and strongly promotes tumor growth and survival through metastasis [25–29]. Interestingly, the activation of the hypoxia-inducible factor HIF1α/heme oxygenase-1 signaling pathway attenuated sepsis-induced acute lung injury and reduced Golgi stress by increasing the expression of Golgi structural proteins such as golgin-97 [30]. We then examined whether HIF1α influences golgin-97 and MAPK signal transduction in breast cancer cells. We detected HIF1α accumulation with increasing doses of $CoCl_2$ but decreased protein levels of golgin-97, TGN46, and IκBα (Fig. 6A-D). Upon incubation with $CoCl_2$, ERK1/2 and

(See figure on next page.)

Fig. 5 Inhibition of ERK/MAPK kinase is effective in overcoming golgin-97 KO-induced tumor growth and lung metastasis. **A** NOD/SCID mice were subcutaneously injected with 2-9 KO cells, followed by veh. control, inhibitor (SB203580+U0126), PTX, or a combination of an inhibitor with PTX (PTX+SB203580+U0126), and tumor growth was monitored. The tumor sizes (cm) are indicated at the bottom. **B** Chart showing tumor sizes and weights from 5A. The data are based on two-way ANOVA. **C** Survival rates of NOD/SCID mice from 5A. Kaplan–Meier plots in which the standard tumor size (300 mm^3) was used as a criterion for euthanasia in the veh.-control and drug treatment groups. **D** Representative images of IHC staining for CD68 in primary tumors. Scale bars, 50 μm. **E** Quantification of CD68-positive cells derived from panel 5D. **F**–**G** qRT–PCR analysis of murine TNFα and TGFβ mRNA levels in primary tumors from mice. The data were analyzed via one-way ANOVA. **H** and **J** Representative images of lung metastasis sections with H&E staining and IHC staining with anti-Ki67 and anti-CD68 antibodies. The yellow arrows delineate the lung metastasis region of the primary tumor. Quantification of Ki67-positive cells (**I**) and CD68-positive cells (**K**) from the lower panel (5H and 5J). The data were analyzed via one-way ANOVA. **L** Western blotting analysis of cleaved caspase-3 and pro-caspase-3 protein levels in the lung tissues of the mice. Actin was used as the internal control. The quantification of protein expression is shown in the lower panel. The data are presented as the means ± SDs (*$p < 0.05$; **$p < 0.01$; ***, $P < 0.001$; ****, $P < 0.0001$)

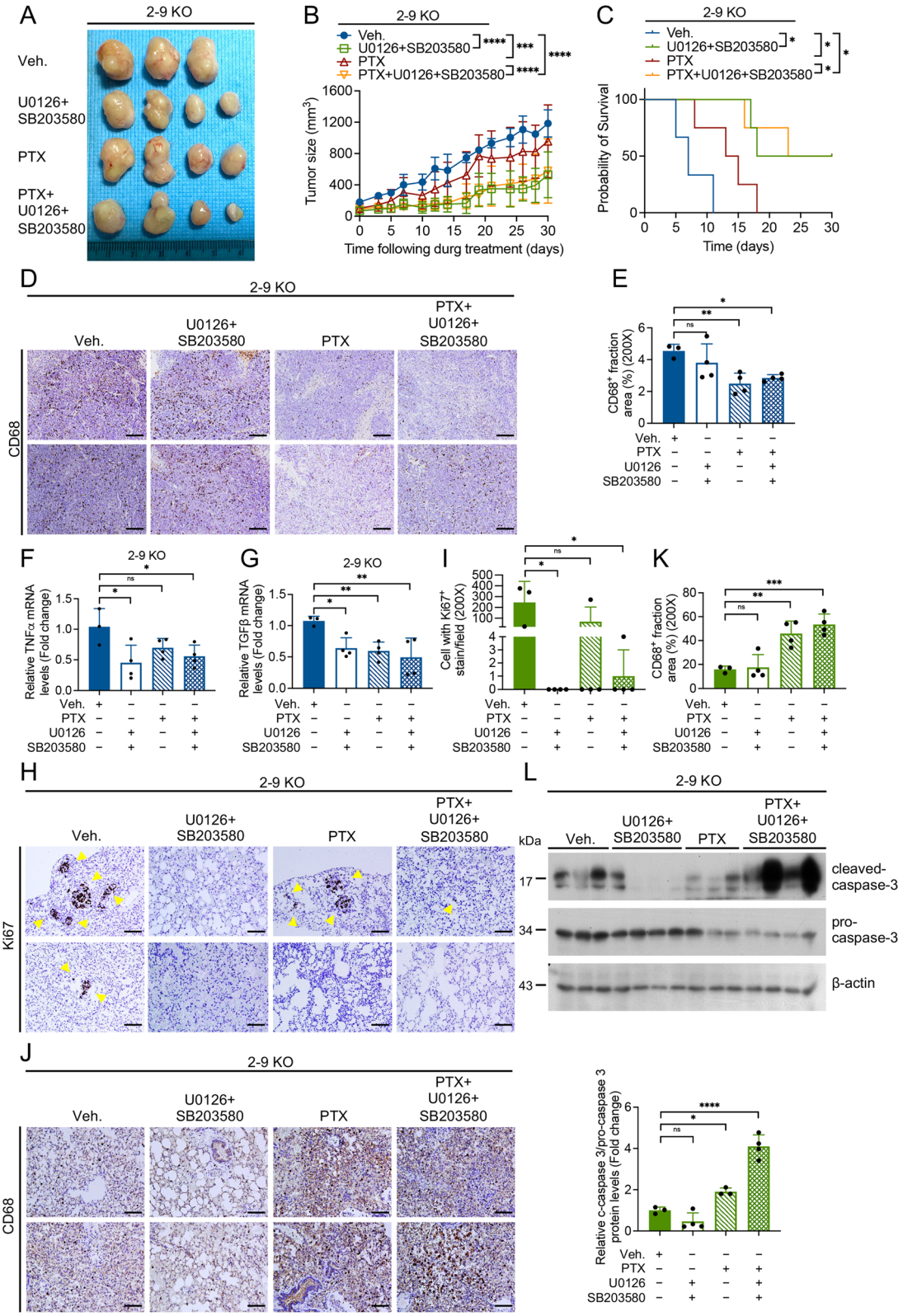

Fig. 5 (See legend on previous page.)

p38 MAPK were activated following the decrease in golgin-97 protein expression (Fig. 6A**, E-F**). These results suggest that, unlike acute lung injury, hypoxia may be a physiological condition that contributes to the downregulation of golgin-97 expression and the activation of ERK/MAPK signaling in cancer cells. Interestingly, treatment of MDA-MB-231 cells with U0126 alone or with two inhibitors (SB203580 + U0126) for 24 h caused a significant increase in golgin-97 protein expression in the MDA-MB-231 cells (Fig. 6G-H). A slight increase (approximately 20%) in golgin-97 mRNA levels was observed in combination-treated cells, suggesting an unexpected mechanism by which MAPK signaling regulates golgin-97 expression at the protein level (Fig. S5A). Consistent with these findings, we also observed an increase in golgin-97 protein but not golgin-97 mRNA expression with single knockdown of ERK1/2 and double knockdown of ERK1/2 and p38 MAPK in MDA-MB-231 and MCF-7 cells (Fig. 6I-L and S5B-3C). These results support the hypothesis that a potential negative regulatory loop exists between ERK/MAPK signaling and golgin-97 expression under hypoxic conditions; therefore, the inhibition of ERK/MAPK may abrogate the tumor-promoting pathways induced by golgin-97 deficiency (Fig. 6M).

Discussion

Accumulating evidence indicates that the Golgi apparatus is a critical regulator of tumor progression. Coiled-coil golgins play a central role in controlling membrane trafficking and act as regulators of Golgi integrity and signal transduction [8, 10, 11, 31, 32]. For example, dysregulation of Golgi-localized Cdc42 signaling by the cis-Golgi matrix protein GM130 may promote the progression of colon and breast cancer [33, 34]. Our recent studies with Kaplan–Meier plotter (http://kmplot.com) and Oncomine (https://www.oncomine.org) data revealed that low golgin-97 expression is correlated with poor survival and increased invasiveness in breast cancer cells [17]. On the basis of the cSurvival database (https://tau.cmmt.ubc.ca/cSurvival/]) and the UALCAN database (https://ualcan.path.uab.edu/), we also observed that low golgin-97 expression significantly worsened the prognosis of progression-free survival ($P = 0.0058$). TCGA data revealed that golgin-97 expression is notably lower in TNBC patients than in normal controls ($P < 1 \times 10^{-12}$), luminal cancer patients ($P = 1.11 \times 10^{-16}$), and HER2-positive patients ($P = 7.39 \times 10^{-4}$) (Fig. S6). These results confirm that low golgin-97 expression is a key feature of TNBC and is linked to poor clinical outcomes. The current study showed that golgin-97 KO can promote the metastatic dissemination and lung colonization of TNBC cells in vivo (in zebrafish and immunodeficient mice). Our orthotopic mouse model studies further confirmed that golgin-97 KO has a positive regulatory effect on primary tumor growth and distant metastasis, accompanied by a proinflammatory tumor microenvironment with features such as increased secretion of murine tumor-associated macrophage-related factors in tumor tissues (Fig. 6M). Macrophages and growth factors/cytokines directly contribute to processes facilitating breast tumor progression and metastasis, including tumor cell growth, migration, invasion, and intravasation [35, 36]. To assess whether inflammatory cytokines or growth factors modulate golgin-97 expression, we administered IL-6, IL-1β, and TGF-β to MDA-MB-231 cells. The results demonstrated that short-term exposure to these cytokines led to a decrease in golgin-97 mRNA expression. Prolonged stimulation with TGF-β alone sustained the reduction in golgin-97 mRNA levels, whereas treatment with IL-6 and IL-1β tended to lead to recovery of golgin-97 mRNA expression. Nonetheless, golgin-97 protein levels increased following stimulation with all three cytokines (Fig. S7). These findings suggest a complex regulatory mechanism involving golgin-97 in response to inflammatory cytokines. Specifically, while short-term exposure to IL-6, IL-1β, and TGF-β reduces golgin-97 mRNA levels, the simultaneous increase in golgin-97 protein expression indicates a potential posttranscriptional regulatory effect. This discrepancy may reflect an adaptive cellular response in which cells prioritize the production or stabilization of golgin-97 protein despite reduced mRNA

(See figure on next page.)

Fig. 6 Hypoxia mimetics and ERK/MAPK signaling regulate golgin-97 expression in breast cancer. **A** MDA-MB-231 cells were treated with increasing concentrations of $CoCl_2$ for 24 h and then subjected to Western blotting analysis with phosphosite- and protein-specific antibodies, as indicated. Actin was used as the internal control. **B**-**F** Quantification of protein expression, as shown in panel 6A. **G** MDA-MB-231 cells treated with kinase inhibitors were prepared for Western blotting analysis via phosphosite- and protein-specific antibodies, as indicated. Actin was used as the internal control. **H** Quantification of golgin-97 protein expression levels from panel 6G. The quantitative data were analyzed via one-way ANOVA. The golgin-97 protein level in MDA-MB-231 cells (**I**) and MCF-7 cells (**J**) following p38 MAPK, ERK1/2 individual knockdown, or combined with double knockdown. **K**, **L** Quantification of golgin-97 protein expression levels from panel 6I–6J. The data were analyzed via one-way ANOVA. The data are presented as the means ± SDs. *$p < 0.05$; **$p < 0.01$; ***, $P < 0.001$ based on one-way ANOVA. **M** Golgin-97 deletion promotes cancer progression, an effect that involves hypoxia, MAPK signaling, and the tumor microenvironment. MAPK inhibitors could be used to suppress golgin-97 deregulation in TNBC. This model is based in part on an illustration from biorender.com

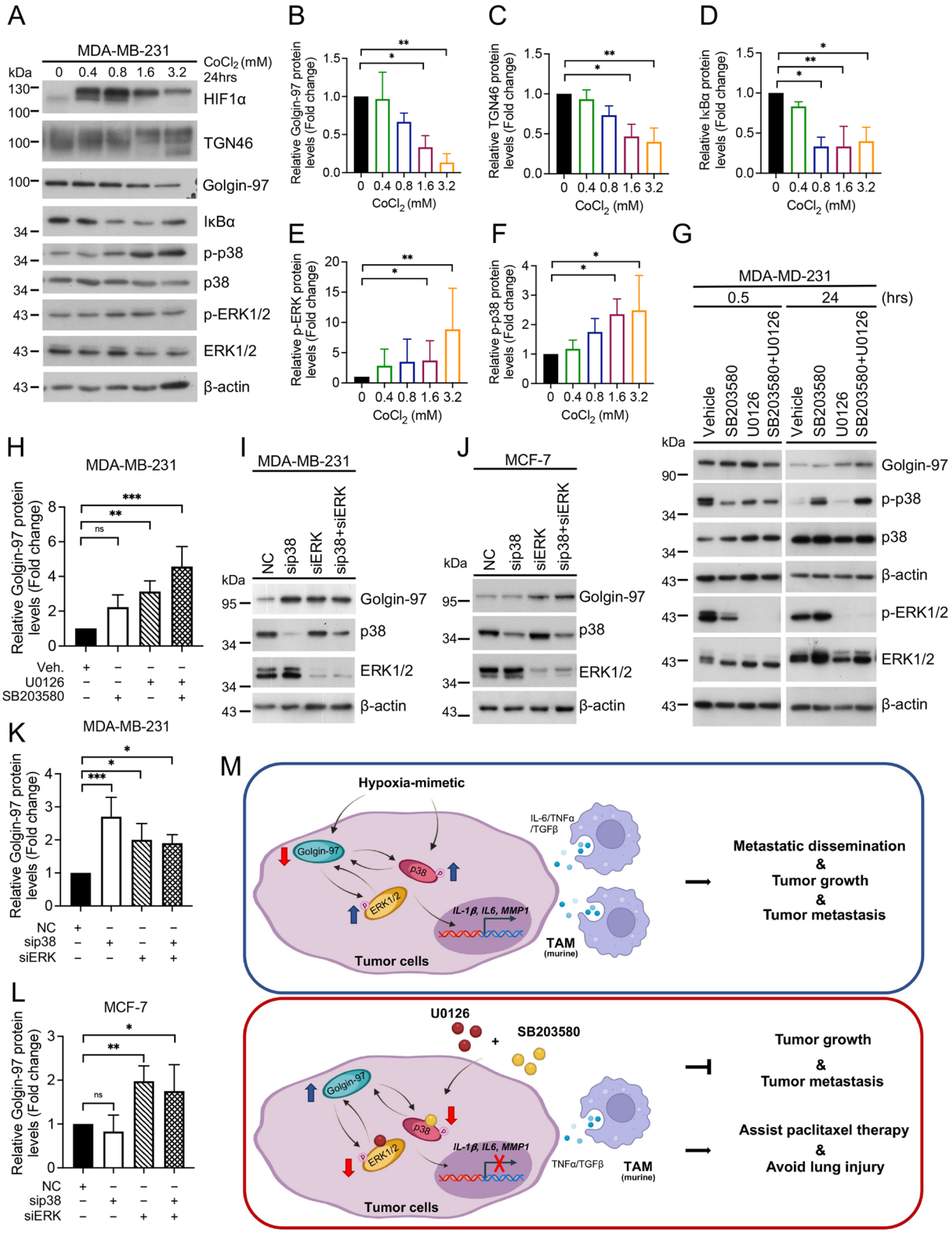

Fig. 6 (See legend on previous page.)

levels, possibly to support functions associated with cellular stress and inflammation. Given that neither the knockdown nor the KO of golgin-97 significantly increased cell proliferation in vitro, we propose that tumor cell–stromal cell interactions have a critical impact during golgin-97 KO-mediated cancer progression.

Currently, drugs targeting Golgi-resident proteins for treating various cancers and metastases have entered clinical trial stages, demonstrating the feasibility and potential of targeting the Golgi apparatus in cancer therapy [37]. However, the challenges remain the specificity of the target, with a significant reduction in complications. Our omics study revealed that the Wnt signaling pathway, MAPK kinase cascades, and inflammatory cytokines are the key regulators that are significantly upregulated in golgin-97 KO cells. Previous studies have reported that individual treatment with the ERK inhibitor U0126 or the p38 MAPK inhibitor SB203580 effectively inhibits the proliferation and invasion of breast cancer cells, but the specific regulatory factors involved remain unclear [38–43]. During cancer progression, activated macrophages can polarize into two major subsets, M1 and M2, which promote tumorigenic capabilities through the secretion of inflammatory cytokines, including TNFα and TGFβ [44]. Although combined treatment with U0126 and SB203580 did not decrease CD68 infiltration in mice derived from golgin-97 KO cells, these two kinase inhibitors significantly reduced murine TNFα and TGFβ expression levels in primary tumors. The current study proposes an intriguing and promising therapeutic strategy: administering ERK/MAPK inhibitors to maintain tumor-suppressing golgin-97 protein expression in TNBC, thereby attenuating breast cancer growth, the inflammatory response, and lung metastasis. Our study also revealed the benefits of ERK/MAPK inhibitors in preventing lung metastasis and lung injury. Specifically, pulmonary drug toxicity is a cause of interstitial lung disease, which can range from benign infiltrates to life-threatening acute respiratory distress syndrome. Direct dose-dependent toxicity and immune inflammation are the main causes of lung damage and fibrosis. We showed that PTX alone but not kinase inhibitors alone caused CD68 infiltration into lung sections and induced lung damage. Severe lung damage occurred when PTX was given in combination with these two inhibitors, suggesting that the drug dosage and/or other unknown signaling pathways contribute to this lung damage. Future work will focus on using mouse breast cancer animal models to reveal the interaction between golgin-97 and specific immune cells and optimize combination treatment strategies for breast cancer.

U0126 is a MEK1/2 inhibitor that primarily targets MEK in the MAP kinase pathway, blocking downstream ERK1/2 signaling and impacting p38 MAPK activity [45]. Notably, low-dose, short-term use of U0126 reduces p38 MAPK phosphorylation, whereas prolonged treatment with both SB203580 and U0126 results in increased phosphorylation of p38 and ERK1/2. This suggests a reciprocal balance between the phosphorylation of ERK and p38, where the inhibition of one pathway leads to an increase in the activity of the other pathway [46, 47]. For example, treatment with high concentrations of SB203580 has been reported to activate Raf-1 and ERK signaling [48, 49], supporting potential crosstalk between ERK and p38 MAPK signaling with SB203580 in cancer therapy. U0126 may inhibit breast cancer growth by blocking the cell cycle, but the role of p38 in cancer remains complex and is currently a subject of ongoing debate [45, 50]. Importantly, our findings support this complexity, aligning with the results presented in Fig. 6G and Fig. 4C, which demonstrated potential crosstalk between U0126 and SB203580. This interaction also strengthens the idea that the combination of these two kinase inhibitors results in antitumor activity in vivo (Fig. 5) while also helping to explain the lack of synergistic effects observed with U0126 and SB203580 in our in vitro assays (Fig. 4).

Our results demonstrated that U0126 and SB203580 individually inhibited the mRNA expression of inflammatory cytokines and MMP1, which was upregulated by golgin-97 KO. The increased IL-6 mRNA levels in 2–9 KO cells after ERK knockdown, as shown in Fig. 4C, may be due to several factors. First, there is a reciprocal relationship between the phosphorylation of ERK and p38 MAPK, where inhibiting one pathway may increase the other [46, 47]. Second, p38 MAPK and IL-6 have a reciprocal and interconnected relationship in several pathways [51]. Third, Wnt5a activates JNK, ERK1/2, and ERK5, contributing to IL-6 expression in preadipocytes [52]. However, loss of ERK1/2 can stimulate ERK5 signaling in epithelial cells, enhancing IL-6 expression in the tumor microenvironment [53]. We noted increased Wnt5a in golgin-97 KO cells (data not shown), potentially increasing ERK5 activity and IL-6 mRNA levels. Therefore, the increase in IL-6 following ERK knockdown is plausible. Compared with U0126, SB203580 alone was insufficient to reduce cell viability but more effectively inhibited the collective migration of golgin-97 KO cells, suggesting that different MAPK signaling pathways may be required for golgin-97 KO-induced cell proliferation and motility (Fig. 6M). The siRNA knockdown results suggest that p38 MAPK and ERK1/2 not only impact golgin-97 protein expression but also modulate cell motility and the cytotoxic effects of chemotherapy. However, we found that SB203580 treatment alone did not increase golgin-97 protein expression, which is

inconsistent with p38 silencing. This inconsistency may be due to the specificity and off-target effects of kinase inhibitors [54]. Treatment with high concentrations of SB203580 has been reported to activate Raf-1 and ERK signaling [48, 49], supporting potential crosstalk between ERK and p38 MAPK signaling with SB203580 in cancer therapy. Consistently, we also observed that combined treatment with U0126 and SB203580 had the most promising effects on cancer progression in golgin-97 KO cells.

We observed that the suppression of p38 MAPK and ERK1/2 increased the protein but not the mRNA expression of golgin-97. ERK reportedly promotes tumorigenesis by regulating protein stability through the ubiquitin–proteasome pathway [55]; thus, MAPK inhibitors may maintain the protein expression of golgin-97 in breast cancer cells. Consistent with this idea, the golgin-97, IκBα, and TGN46 protein levels were reduced, but ERK and p38 MAPK were activated in $CoCl_2$-treated cells, indicating an inverse correlation between golgin-97 expression and MAPK signaling activity (Fig. 6M). Given that $CoCl_2$-induced HIF1α expression occurs mainly through ERK and p38 MAPK activation [56, 57], we cannot exclude the possibility that ERK and p38 MAPK signaling may be upstream regulators of golgin-97. These findings also support the possibility of a feedback loop between MAPKs and golgin-97 in the modulation of breast cancer progression under hypoxic conditions. Additionally, we found that IL-1β levels were increased in golgin-97 KO cells. IL-1β mainly regulates cell migration by activating p38 MAPK, and its substrate MAPKAPK2 is involved in modulating the tumor microenvironment, thereby further promoting the invasion of breast cancer cells [58, 59]. IL-1β-induced migration of MDA-MB-231 cells under hypoxic conditions has also been reported [60]. By using a hypoxic chamber, we found that the protein levels of golgin-97 were increased in MDA-MB231 cells under short-term hypoxia treatment (15 min), whereas golgin-97 and TGN46 were significantly decreased after 2 to 8 h of hypoxic exposure (data not shown). The current study reports the interplay between hypoxia and the golgin-97 and MAPK signaling pathways. However, further studies are needed to determine whether this mechanism is directly mediated by golgin-97 in vivo. Nevertheless, we hypothesize that hypoxia and exposure to unidentified stimulators are the physiological conditions involved in golgin-97 downregulation, which modulates the tumor microenvironment and promotes cell aggressiveness in vivo.

To our knowledge, our study is the first to report that golgin-97 affects tumor growth and metastasis possibly through communication between cancer cells and inflammatory stromal cells. Both the anti-inflammatory effects and the restoration of tumor-suppressive golgin-97 expression contribute to the efficacy of U0126 and SB203580 kinase inhibitors in breast cancer therapy. Compared with the paclitaxel regimen, these two kinase inhibitors have the potential to prevent lung injury. Although golgin-97 does not have kinase activity or directly affects protein stability, we propose that it may indirectly affect signaling pathways such as the ERK1/2 and p38 MAPK pathways for three reasons. First, golgin-97 aids in transport and organization within the TGN, helping to sort signaling molecules and receptors [61]. By ensuring correct localization, golgin-97 can alter protein activation in signaling pathways. Second, as a tethering factor, it promotes vesicle fusion and affects access to growth factor or cytokine receptors, such as IL-10 [62, 63]. Third, changes in Golgi integrity, especially in cancer cells, can disrupt the processing and glycosylation of signaling molecules, significantly altering receptor signaling and activation of the ERK1/2 and p38 MAPK pathways [64]. Investigations of the impact of golgin-97 on different cancers are rare, and more evidence is needed to explore its clinical application. Overall, this study provides new therapeutic strategies for TNBC and may benefit drug development.

Abbreviations

TNBC	Triple-negative breast cancer
KO	Knockout
PTX	Paclitaxel
$CoCl_2$	Cobalt chloride
DMSO	Dimethyl sulfoxide
CCK-8	Cell Counting Kit-8
MAPK	Mitogen-activated protein kinase
TNF	Tumor necrosis factor
TGN	*Trans*-Golgi network
ERK	Extracellular signal-regulated kinase
MEK	MAPK/extracellular signal-regulated kinase
HIF1α	Hypoxia-inducible factor 1 alpha
IL-1β	Interleukin 1 beta
IL-6	Interleukin 6
TGFβ	Transforming growth factor beta
MMP-1	Matrix metalloproteinase-1
NF-κB	Nuclear factor kappa-B
qPCR	Quantitative PCR; RT–PCR, reverse transcription polymerase chain reaction
TMT	Tandem mass tag
2D LC–MS/MS	Two-dimensional liquid chromatography–tandem mass spectrometry
NGS	Next-generation sequencing
IPA	Ingenuity Pathway Analysis
DEGs	Differentially expressed genes
DAVID	Database for Annotation, Visualization and Integrated Discovery
WT	Wild-type
SDs	Standard deviations

Supplementary Information

The online version contains supplementary material available at https://doi.org/10.1186/s12964-024-02010-0.

The online version contains Appendix S1, Supplementary Figures S1-S7, and Supplementary Tables S1-S3. All the data are contained within the article and/or the supporting information. The mass spectrometry proteomics data have been deposited to the ProteomeXchange Consortium via the PRIDE partner repository [65] with the dataset identifier PXD056499.

Additional file 1.

Additional file 2.

Additional file 3.

Acknowledgements
We thank Ke-Wei Lin for the technical support in our genomic analysis. We also appreciate Professor Chia-Rui Shen for providing the essential reagents for the co-culture of cancer cells with monocytic cells.

Authors' contributions
Y-C Liu contributed to the design of the experiments, performed the research, analyzed the results, wrote the manuscript draft and revised the manuscript; T-J Lin performed the research, analyzed the results and wrote the manuscript draft; K-Y Chong contributed to the design of the experiments and performed the research; G-Y Chen performed the research and analyzed the results; C-Y Kuo performed the research and analyzed the results; Y-Y Lin performed the research and analyzed the results; C-W Chang helped establish the zebrafish model; T-F Hsiao performed the proteomic analysis; C-L Wang provided the methodology; Y-C Shih performed the research and contributed to the data analysis; and C-J Yu was responsible for conceptualization, experimental design, supervision, writing, review & editing, and funding acquisition.

Data availability
The mass spectrometry proteomics data have been deposited to the ProteomeXchange Consortium via the PRIDE partner repository with the dataset identifier PXD056499 (http://www.ebi.ac.uk/pride).

Declarations

Ethics approval and consent to participate
The animal protocol was reviewed and approved by the Laboratory Animal Use Committee of Chang Gung University (CGU107-228).

Competing interests
The authors declare no competing interests.

Author details
[1]Department of Cell and Molecular Biology, College of Medicine, Chang Gung University, 259 Wen-Hwa 1 road, Guishan District, Taoyuan, Taiwan. [2]CardioVascular Research Center, Tzu Chi General Hospital, Hualien City, Hualien County, Taiwan. [3]Department of Medical Biotechnology and Laboratory Sciences, College of Medicine, Chang Gung University, Taoyuan, Taiwan. [4]Graduate Institute of Biomedical Sciences Division of Biotechnology, College of Medicine, Chang Gung University, Taoyuan, Taiwan. [5]Hyperbaric Oxygen Medical Research Lab, Bone and Joint Research Center, Linkou Chang Gung Memorial Hospital, Taoyuan, Taiwan. [6]Centre for Stem Cell Research, Faculty of Medicine and Health Sciences, Universiti Tunku Abdul Rahman, Selangor, Malaysia. [7]Graduate Institute of Biomedical Sciences, College of Medicine, Chang Gung University, Taoyuan, Taiwan. [8]School of Medicine, College of Medicine, Chang Gung University, Taoyuan, Taiwan. [9]Department of Thoracic Medicine, Chang Gung Memorial Hospital, Taoyuan, Taiwan. [10]Molecular Medicine Research Center, Chang Gung University, Taoyuan, Taiwan.

Received: 22 October 2024 Accepted: 22 December 2024
Published online: 13 January 2025

References

1. DeSantis CE, Ma J, Goding Sauer A, Newman LA, Jemal A. Breast cancer statistics, 2017, racial disparity in mortality by state. CA Cancer J Clin. 2017;67:439–48.
2. Chavez KJ, Garimella SV, Lipkowitz S. Triple negative breast cancer cell lines: one tool in the search for better treatment of triple negative breast cancer. Breast Dis. 2010;32:35–48.
3. Obidiro O, Battogtokh G, Akala EO. Triple Negative Breast Cancer Treatment Options and Limitations: Future Outlook. Pharmaceutics. 2023;15:1796.
4. Bielopolski D, Evron E, Moreh-Rahav O, Landes M, Stemmer SM, Salamon F. Paclitaxel-induced pneumonitis in patients with breast cancer: case series and review of the literature. J Chemother. 2017;29:113–7.
5. Limpawittayakul P, Petchjorm S, Chueansuwan W, Boonfueang W. Paclitaxel-induced acute fibrinous and organizing pneumonitis in early breast cancer: A case report. Respir Med Case Rep. 2024;48: 102004.
6. Mohan N, Dalip D, Rampersad FS, Jaggernauth S. Paclitaxel-Induced Pneumonitis in Trinidad: A Case Report. Cureus. 2022;14: e26613.
7. Makaraci P, Kim K. trans-Golgi network-bound cargo traffic. Eur J Cell Biol. 2018;97:137–49.
8. Millarte V, Farhan H. The Golgi in cell migration: regulation by signal transduction and its implications for cancer cell metastasis. ScientificWorldJournal. 2012;2012: 498278.
9. Bajaj R, Warner AN, Fradette JF, Gibbons DL. Dance of The Golgi: Understanding Golgi Dynamics in Cancer Metastasis. Cells. 2022;11:1484.
10. Spano D, Colanzi A. Golgi Complex: A Signaling Hub in Cancer. Cells 2022; 11.
11. Bui S, Mejia I, Diaz B, Wang Y. Adaptation of the Golgi Apparatus in Cancer Cell Invasion and Metastasis. Front Cell Dev Biol. 2021;9: 806482.
12. Griffith KJ, Chan EK, Lung CC, Hamel JC, Guo X, Miyachi K, Fritzler MJ. Molecular cloning of a novel 97-kd Golgi complex autoantigen associated with Sjögren's syndrome. Arthritis Rheum. 1997;40:1693–702.
13. Lock JG, Hammond LA, Houghton F, Gleeson PA, Stow JL. E-cadherin transport from the trans-Golgi network in tubulovesicular carriers is selectively regulated by golgin-97. Traffic. 2005;6:1142–56.
14. Munro S, Nichols BJ. The GRIP domain - a novel Golgi-targeting domain found in several coiled-coil proteins. Curr Biol. 1999;9:377–80.
15. Yu CJ, Lee FJ. Multiple activities of Arl1 GTPase in the trans-Golgi network. J Cell Sci. 2017;130:1691–9.
16. Radvanyi L, Singh-Sandhu D, Gallichan S, Lovitt C, Pedyczak A, Mallo G, Gish K, Kwok K, Hanna W, Zubovits J, et al. The gene associated with trichorhinophalangeal syndrome in humans is overexpressed in breast cancer. Proc Natl Acad Sci U S A. 2005;102:11005–10.
17. Hsu RM, Zhong CY, Wang CL, Liao WC, Yang C, Lin SY, Lin JW, Cheng HY, Li PY, Yu CJ. Golgi tethering factor golgin-97 suppresses breast cancer cell invasiveness by modulating NF-κB activity. Cell Commun Signal. 2018;16:19.
18. Lin Y, Bai L, Chen W, Xu S. The NF-kappaB activation pathways, emerging molecular targets for cancer prevention and therapy. Expert Opin Ther Targets. 2010;14:45–55.
19. Veinotte CJ, Dellaire G, Berman JN. Hooking the big one: the potential of zebrafish xenotransplantation to reform cancer drug screening in the genomic era. Dis Model Mech. 2014;7:745–54.
20. Liao WC, Lin TJ, Liu YC, Wei YS, Chen GY, Feng HP, Chang YF, Chang HT, Wang CL, Chi HC, et al. Nuclear accumulation of KPNA2 impacts radioresistance through positive regulation of the PLSCR1-STAT1 loop in lung adenocarcinoma. Cancer Sci. 2022;113:205–20.
21. Bardi GT, Smith MA, Hood JL. Melanoma exosomes promote mixed M1 and M2 macrophage polarization. Cytokine. 2018;105:63–72.
22. Carata E, Muci M, Mariano S, Di Giulio S, Nigro A, Romano A, Panzarini E. Extracellular Vesicles from NSC-34 MN-like Cells Transfected with Mutant SOD1 Modulate Inflammatory Status of Raw 264.7 Macrophages. Genes (Basel) 2024;15.
23. Crown J, O'Leary M, Ooi WS. Docetaxel and paclitaxel in the treatment of breast cancer: a review of clinical experience. Oncologist. 2004;9(Suppl 2):24–32.
24. Gradishar WJ. Taxanes for the treatment of metastatic breast cancer. Breast Cancer (Auckl). 2012;6:159–71.
25. Zhang J, Ouyang F, Gao A, Zeng T, Li M, Li H, Zhou W, Gao Q, Tang X, Zhang Q, et al. ESM1 enhances fatty acid synthesis and vascular mimicry in ovarian cancer by utilizing the PKM2-dependent warburg effect within the hypoxic tumor microenvironment. Mol Cancer. 2024;23:94.

26. Karagiota A, Kourti M, Simos G, Mylonis I. HIF-1alpha-derived cell-penetrating peptides inhibit ERK-dependent activation of HIF-1 and trigger apoptosis of cancer cells under hypoxia. Cell Mol Life Sci. 2019;76:809–25.
27. Kong R, Wei W, Man Q, Chen L, Jia Y, Zhang H, Liu Z, Cheng K, Mao C, Liu S. Hypoxia-induced circ-CDYL-EEF1A2 transcriptional complex drives lung metastasis of cancer stem cells from hepatocellular carcinoma. Cancer Lett. 2023;578: 216442.
28. Chen Z, Han F, Du Y, Shi H, Zhou W. Hypoxic microenvironment in cancer: molecular mechanisms and therapeutic interventions. Signal Transduct Target Ther. 2023;8:70.
29. Jing X, Yang F, Shao C, Wei K, Xie M, Shen H, Shu Y. Role of hypoxia in cancer therapy by regulating the tumor microenvironment. Mol Cancer. 2019;18:157.
30. Li X, Yu J, Gong L, Zhang Y, Dong S, Shi J, Li C, Li Y, Zhang Y, Li H. Heme oxygenase-1(HO-1) regulates Golgi stress and attenuates endotoxin-induced acute lung injury through hypoxia inducible factor-1alpha (HIF-1alpha)/HO-1 signaling pathway. Free Radic Biol Med. 2021;165:243–53.
31. Lu L, Tai G, Hong W. Autoantigen Golgin-97, an effector of Arl1 GTPase, participates in traffic from the endosome to the trans-golgi network. Mol Biol Cell. 2004;15:4426–43.
32. Yadav S, Puri S, Linstedt AD. A primary role for Golgi positioning in directed secretion, cell polarity, and wound healing. Mol Biol Cell. 2009;20:1728–36.
33. Baschieri F, Confalonieri S, Bertalot G, Di Fiore PP, Dietmaier W, Leist M, Crespo P, Macara IG, Farhan H. Spatial control of Cdc42 signalling by a GM130-RasGRF complex regulates polarity and tumorigenesis. Nat Commun. 2014;5:4839.
34. Baschieri F, Uetz-von Allmen E, Legler DF, Farhan H. Loss of GM130 in breast cancer cells and its effects on cell migration, invasion and polarity. Cell Cycle. 2015;14:1139–47.
35. Condeelis J, Pollard JW. Macrophages: obligate partners for tumor cell migration, invasion, and metastasis. Cell. 2006;124:263–6.
36. Tang XQ. Tumor-associated macrophages as potential diagnostic and prognostic biomarkers in breast cancer. Cancer Lett. 2013;332:3–10.
37. Zappa F, Failli M, De Matteis MA. The Golgi complex in disease and therapy. Curr Opin Cell Biol. 2018;50:102–16.
38. Uehara N, Matsuoka Y, Tsubura A. Mesothelin promotes anchorage-independent growth and prevents anoikis via extracellular signal-regulated kinase signaling pathway in human breast cancer cells. Mol Cancer Res. 2008;6:186–93.
39. Yang F, Tang XY, Liu H, Jiang ZW. Inhibition of mitogen-activated protein kinase signaling pathway sensitizes breast cancer cells to endoplasmic reticulum stress-induced apoptosis. Oncol Rep. 2016;35:2113–20.
40. Duzgun SA, Yerlikaya A, Zeren S, Bayhan Z, Okur E, Boyaci I. Differential effects of p38 MAP kinase inhibitors SB203580 and SB202190 on growth and migration of human MDA-MB-231 cancer cell line. Cytotechnology. 2017;69:711–24.
41. He Q, Xue S, Tan Y, Zhang L, Shao Q, Xing L, Li Y, Xiang T, Luo X, Ren G. Dual inhibition of Akt and ERK signaling induces cell senescence in triple-negative breast cancer. Cancer Lett. 2019;448:94–104.
42. Ren J, Wang Y, Ware T, Iaria J, Ten Dijke P, Zhu HJ. Reactivation of BMP signaling by suboptimal concentrations of MEK inhibitor and FK506 reduces organ-specific breast cancer metastasis. Cancer Lett. 2020;493:41–54.
43. Wang Z, Wang F, Ding XY, Li TE, Wang HY, Gao YH, Wang WJ, Liu YF, Chen XS, Shen KW. Hippo/YAP signaling choreographs the tumor immune microenvironment to promote triple negative breast cancer progression via TAZ/IL-34 axis. Cancer Lett. 2022;527:174–90.
44. Zhang Q, Sioud M. Tumor-Associated Macrophage Subsets: Shaping Polarization and Targeting. Int J Mol Sci 2023;24.
45. You Y, Niu Y, Zhang J, Huang S, Ding P, Sun F, Wang X. U0126: Not only a MAPK kinase inhibitor. Front Pharmacol. 2022;13: 927083.
46. Hotokezaka H, Sakai E, Kanaoka K, Saito K, Matsuo K, Kitaura H, Yoshida N, Nakayama K. U0126 and PD98059, specific inhibitors of MEK, accelerate differentiation of RAW264.7 cells into osteoclast-like cells. J Biol Chem 2002; 277**:**47366–47372.
47. Poddar R, Paul S. Novel crosstalk between ERK MAPK and p38 MAPK leads to homocysteine-NMDA receptor-mediated neuronal cell death. J Neurochem. 2013;124:558–70.
48. Birkenkamp KU, Tuyt LM, Lummen C, Wierenga AT, Kruijer W, Vellenga E. The p38 MAP kinase inhibitor SB203580 enhances nuclear factor-kappa B transcriptional activity by a non-specific effect upon the ERK pathway. Br J Pharmacol. 2000;131:99–107.
49. Feng L, Xie X, Ding Q, Luo X, He J, Fan F, Liu W, Wang Z, Chen Y. Spatial regulation of Raf kinase signaling by RKTG. Proc Natl Acad Sci U S A. 2007;104:14348–53.
50. Low HB, Zhang Y. Regulatory Roles of MAPK Phosphatases in Cancer. Immune Netw. 2016;16:85–98.
51. Krupkova O, Sadowska A, Kameda T, Hitzl W, Hausmann ON, Klasen J, Wuertz-Kozak K. p38 MAPK Facilitates Crosstalk Between Endoplasmic Reticulum Stress and IL-6 Release in the Intervertebral Disc. Front Immunol. 2018;9:1706.
52. Díaz-Chamorro S, Garrido-Jiménez S, Barrera-López JF, Mateos-Quirós CM, Cumplido-Laso G, Lorenzo MJ, Román ÁC, Bernardo E, Sabio G, Carvajal-González JM, Centeno F. Title: p38δ Regulates IL6 Expression Modulating ERK Phosphorylation in Preadipocytes. Front Cell Dev Biol. 2021;9: 708844.
53. de Jong PR, Taniguchi K, Harris AR, Bertin S, Takahashi N, Duong J, Campos AD, Powis G, Corr M, Karin M, Raz E. ERK5 signalling rescues intestinal epithelial turnover and tumour cell proliferation upon ERK1/2 abrogation. Nat Commun. 2016;7:11551.
54. Weiss WA, Taylor SS, Shokat KM. Recognizing and exploiting differences between RNAi and small-molecule inhibitors. Nat Chem Biol. 2007;3:739–44.
55. Yang JY, Zong CS, Xia W, Yamaguchi H, Ding Q, Xie X, Lang JY, Lai CC, Chang CJ, Huang WC, et al. ERK promotes tumorigenesis by inhibiting FOXO3a via MDM2-mediated degradation. Nat Cell Biol. 2008;10:138–48.
56. Chen R, Xu J, She Y, Jiang T, Zhou S, Shi H, Li C. Necrostatin-1 protects C2C12 myotubes from CoCl2-induced hypoxia. Int J Mol Med. 2018;41:2565–72.
57. Wang G, Li Y, Yang Z, Xu W, Yang Y, Tan X. ROS mediated EGFR/MEK/ERK/HIF-1alpha Loop Regulates Glucose metabolism in pancreatic cancer. Biochem Biophys Res Commun. 2018;500:873–8.
58. Gelfo V, Romaniello D, Mazzeschi M, Sgarzi M, Grilli G, Morselli A, Manzan B, Rihawi K, Lauriola M. Roles of IL-1 in Cancer: From Tumor Progression to Resistance to Targeted Therapies. Int J Mol Sci. 2020;21:6009.
59. Rebe C, Ghiringhelli F. Interleukin-1beta and Cancer. Cancers (Basel). 2020;12:1791.
60. Filippi I, Carraro F, Naldini A. Interleukin-1β Affects MDAMB231 Breast Cancer Cell Migration under Hypoxia: Role of HIF-1α and NFκB Transcription Factors. Mediators Inflamm. 2015;2015: 789414.
61. Shin JJH, Crook OM, Borgeaud AC, Cattin-Ortolá J, Peak-Chew SY, Breckels LM, Gillingham AK, Chadwick J, Lilley KS, Munro S. Spatial proteomics defines the content of trafficking vesicles captured by golgin tethers. Nat Commun. 2020;11:5987.>
62. Stanley AC, Lieu ZZ, Wall AA, Venturato J, Khromykh T, Hamilton NA, Gleeson PA, Stow JL. Recycling endosome-dependent and -independent mechanisms for IL-10 secretion in LPS-activated macrophages. J Leukoc Biol. 2012;92:1227–39.
63. Murray RZ, Stow JL. Cytokine Secretion in Macrophages: SNAREs, Rabs, and Membrane Trafficking. Front Immunol. 2014;5:538.
64. Li Y, Mu L, Li Y, Mi Y, Hu Y, Li X, Tao D, Qin J. Golgi dispersal in cancer stem cells promotes chemoresistance of colorectal cancer via the Golgi stress response. Cell Death Dis. 2024;15:417.
65. Griss J, Perez-Riverol Y, Lewis S, Tabb DL, Dianes JA, Del-Toro N, Rurik M, Walzer MW, Kohlbacher O, Hermjakob H, et al. Recognizing millions of consistently unidentified spectra across hundreds of shotgun proteomics datasets. Nat Methods. 2016;13:651–6.

Publisher's Note